Supplemental Material: Multi-Scale Data-Driven Modeling and Observation of Calcium Puffs

Ghanim Ullah[a], Ian Parker[b],
Don-On Daniel Mak[c], and John E Pearson[a]

[a]Theoretical Biology and Biophysics, Los Alamos National Laboratory,
Los Alamos, New Mexico;
[b]Departments of Neurobiology and Behavior,
Physiology and Biophysics, University of California,
Irvine, California;
[c] Department of Physiology, University of Pennsylvania,
Philadelphia, Pennsylvania

1 Supplemental Methods

1.1 Seven State Single Channel Model With IP_3 Dependence

The P_O and other kinetics of IP_3R change with C and I. The peak P_O increases nonlinearly as we increase I (symbols in Figure 2S). To reach a minimal model that gives both the IP_3 and Ca^{2+} dependence of IP_3R gating we fit the open probability function to the P_O data where P_O is a function of both C and I. Using the information criterion proposed by Scharz [1] we find that the best fit to the P_O data is obtained by using the following rational function in both C and I. Note that the "best fit" here refers to the fit to the P_O data that depends on both C and I, while in case of four state model it refers to the fit to the P_O data at fixed $I = 10\mu M$ and varying C.

$$P_O(C,I) = \frac{K_{O24}C^2I^4}{Z(C,I)} \tag{1S}$$

$$Z(C,I) = K_{R00} + K_{A20}C^2 + K_{I50}C^5 + K_{R04}I^4 + K_{A24}C^2I^4 + K_{O24}C^2I^4 + K_{I54}C^5I^4 \qquad (2S)$$

If the channel kinetics obey the laws of detailed balance and mass action, at least one state can be associated with each distinct monomial in the $P_{\mathbf{O}}$. The monomials are: K_{R00}, $K_{A20}C^2$, $K_{I50}C^5$, $K_{R04}I^4$, $K_{A24}C^2I^4$, $K_{O24}C^2I^4$, and $K_{I54}C^5I^4$. Thus there are seven states: R00, A20, I50, R04, A24, O24, and I54. The first and second indices in each state respectively correspond to the number of C and I bound to the channel when in that state. The constant $K_{\mathbf{X}ij}$ is the product of forward equilibrium constants along any path connecting the rest state R00 to state Xij. We call $K_{\mathbf{X}ij}$ the occupancy parameter of state Xij. The quantity $K_{\mathbf{X}ij}C^iI^j$ is the occupancy of state (Xij) relative to the state R00. The occupancy parameters for the seven states are given in Table 1S.

The model scheme with seven states that explicitly treats Ca^{2+} and IP_3 binding is shown in Figure 1S. Model fit to the experimental data is shown by solid lines in Figure 2S. The patch clamp $P_{\mathbf{O}}$ data given by symbols in Figure 2S is the mean of multiple patch clamp experiments on *Xenopus Laevis* occytes for the same ligand concentrations C and I.

As we will discuss in detail bellow and in the main text in relation to the four state model, there are "low occupancy" states with one, two, and three IP_3 bound that mediates the transition between the rest state **R00**, which has no IP_3 bound, and state **R04**, which has four IP_3 bound. Similarly, there are three low occupancy states for each **A20** $\leftrightharpoons$ **A24** and **I50** $\leftrightharpoons$ **I54** transitions. The $P_{\mathbf{O}}$ data are not adequate to provide accurate estimates of the occupancy of these states, however, they serve as "speed bumps" for the probability flux between high occupancy states.

1.2 Derivation of Transition Rates and Simplification of Four State Model

The transition between the $\mathbf{R}_0$ and $\mathbf{A}_2$ states involve one low occupancy state, $\mathbf{A}_1$. We use the subscripts to represent the number of Ca^{2+} ions bound to IP_3R in that state. To simplify this chain we first write it in terms of probability fluxes as shown in eq. 3S. The probability flux between two states with l and m number of ligands bound respectively is given by $k_{lm}^{flux}C^n$ where k_{lm}^{flux} is the flux parameter and n is the maximum of l and m. The goal is to aggregate this 3 state chain into 2 state chain by eliminating the low occupancy state. We will derive the mean time to go from one state to another. The effective transition rates between the high occupancy states are simply the inverse of mean times to transition

between those states.

$$\mathbf{R_0} \overset{k_{01}^{flux} C}{\Longleftrightarrow} \mathbf{A_1} \overset{k_{12}^{flux} L^2}{\Longleftrightarrow} \mathbf{A_2} \tag{3S}$$

Assuming detailed balance, we can write the generator matrix, Q, in the following form [2, 3]

$$Q = W^{-1} Q^{ef}. \tag{4S}$$

Writing the generator matrix in this form automatically imposes detail balance on the network. W in equation (4S) is the diagonal matrix whose entries are the unnormalized equilibrium occupancies of the three states, $\mathbf{R}_0$, $\mathbf{A}_1$,and $\mathbf{A}_2$.

$$W = \begin{pmatrix} 1 & 0 & 0 \\ 0 & K_{A1}C & 0 \\ 0 & 0 & K_A C^2 \end{pmatrix} \tag{5S}$$

where $K_{A1}C$ and $K_A C^2$ are the occupancies of states $\mathbf{A}_1$ and $\mathbf{A}_2$ respectively relative to state $\mathbf{R}_0$ having an occupancy of 1. We call the constant K_i as the occupancy parameter. Q^{ef} in equation (4S) is the symmetric generator matrix with element Q_{xy}^{ef} corresponding to the equilibrium probability flux from state x to y. The diagonal entries of Q^{ef} are given by $Q_{xx}^{ef} = -\sum_{y \neq x} Q_{xy}^{ef}$ which is an expression of conservation of probability [2].

$$Q^{ef} = \begin{pmatrix} -k_{01}^{flux} C & k_{01}^{flux} C & 0 \\ k_{01}^{flux} C & -k_{01}^{flux} C - k_{12}^{flux} C^2 & k_{12}^{flux} C^2 \\ 0 & k_{12}^{flux} C^2 & -k_{12}^{flux} C^2 \end{pmatrix} \tag{6S}$$

Equations (4S-6S) give

$$Q = \begin{pmatrix} -k_{01}^{flux} C & k_{01}^{flux} C & 0 \\ \frac{k_{01}^{flux}}{K_{A1}} & -\frac{k_{01}^{flux} + k_{12}^{flux} C}{K_{A1}} & \frac{k_{12}^{flux} C}{K_{A1}} \\ 0 & \frac{k_{12}^{flux}}{K_A} & -\frac{k_{12}^{flux}}{K_A} \end{pmatrix} \tag{7S}$$

We first aggregate $\mathbf{R}_0$ and $\mathbf{A}_1$ states and represent the aggregated state by $\mathcal{R}$. The exact distribution of first passage time to go from $\mathcal{R}$ to $\mathbf{A}_2$ is given by

$$f_{\mathcal{R}A_2} = \Pi_{\mathcal{R}} e^{Q_{\mathcal{R}\mathcal{R}}t} Q_{\mathcal{R}A_2} u_{A_2} \tag{8S}$$

where $\Pi_{\mathcal{R}} = \Big(1, 0\Big)$ is a vector whose elements are initial probabilities of states $\mathbf{R}_0$ and $\mathbf{A}_1$ and u_{A_2} is a vector with all entries equal to one and dimension equal to the number of final states to which the system is about to transition, in this case one state (A_2). $Q_{\mathcal{R}\mathcal{R}}$, and $Q_{\mathcal{R}A_2}$ are the sub-matrices of Q

$$Q^{\mathcal{R}\mathcal{R}} = \begin{pmatrix} -k_{01}^{flux} C & k_{01}^{flux} C \\ \frac{k_{01}^{flux}}{K_{A1}} & -\frac{k_{01}^{flux} + k_{12}^{flux} C}{K_{A1}} \end{pmatrix} \tag{9S}$$

$$Q^{\mathcal{R}A_2} = \begin{pmatrix} 0 \\ \frac{k_{12}^{flux} C}{K_{A1}} \end{pmatrix} \tag{10S}$$

We can calculate the mean time to go from aggregated state $\mathcal{R}$ to $\mathbf{A}_2$, $T_{R_o A_2}$, by integrating equation (8S) and is given by

$$T_{R_0 A_2} = \Pi_{\mathcal{R}} (Q_{\mathcal{R}\mathcal{R}})^{-2} Q_{\mathcal{R}A_2} u_{A_2} \tag{11S}$$

$$T_{R_0 A_2} = \frac{k_{01}^{flux} + k_{01}^{flux} K_{A1} C + k_{12}^{flux} C}{k_{01}^{flux} k_{12}^{flux} C^2} \tag{12S}$$

$$T_{R_0 A_2} = \frac{1}{k_{01}^{flux} C} + \frac{1}{k_{12}^{flux} C^2} \tag{13S}$$

The last expression is reached by assuming that the occupancy of the state $\mathbf{A}_1$ is negligible as compared to states $\mathbf{R}_0$ and $\mathbf{A}_2$.

Similarly, the distribution of first passage time to go to $\mathbf{R}_0$ from $\mathcal{A}$, which represents the

aggregate of $\mathbf{A}_1$ and $\mathbf{A}_2$ states is given by

$$f_{\mathcal{A}R_0} = \Pi_{\mathcal{A}} e^{Q_{\mathcal{A}\mathcal{A}} t} Q_{\mathcal{A}R_0} u_{R_0}, \tag{14S}$$

where $\Pi^{\mathcal{A}} = \begin{pmatrix} 0, 1 \end{pmatrix}$ is the row matrix having the initial probabilities of states $\mathbf{A}_1$ and $\mathbf{A}_2$ respectively, u_{R_0} is a 1×1 identity matrix, $Q^{\mathcal{A}\mathcal{A}}$, and $Q^{\mathcal{A}R_0}$ are the sub-matrices of Q

$$Q^{\mathcal{A}\mathcal{A}} = \begin{pmatrix} -\frac{k_{01}^{flux} + k_{12}^{flux} C}{K_{A1}} & \frac{k_{12}^{flux} L}{K_{A1}} \\ \frac{k_{12}^{flux}}{K_A} & -\frac{k_{12}^{flux}}{K_A} \end{pmatrix} \tag{15S}$$

$$Q^{\mathcal{A}R_0} = \begin{pmatrix} \frac{k_{01}^{flux}}{K_{A1}} \\ 0 \end{pmatrix} \tag{16S}$$

Integrating equation (14S) gives us the mean time to go from state $\mathcal{A}$ to $\mathbf{R}_0$ as

$$T_{A_2 R_0} = \Pi^{\mathcal{A}} (Q^{\mathcal{A}\mathcal{A}})^{-2} Q^{\mathcal{A}R_0} u_{R_0} \tag{17S}$$

$$T_{A_2 R_0} = \frac{k_{12}^{flux} K_{A1} + k_{01}^{flux} K_A + k_{12}^{flux} K_A L}{k_{01}^{flux} k_{12}^{flux}} \tag{18S}$$

$$T_{A_2 R_0} = K_A C^2 \left(\frac{1}{k_{01}^{flux} C} + \frac{1}{k_{12}^{flux} C^2} \right) = K_A C^2 T_{R_0 A_2} \tag{19S}$$

Thus we can write

$$T_{RA} = \frac{1}{k_{12}^{flux} C^2} + \frac{1}{k_{01}^{flux} C} \tag{20S}$$

$$T_{AR} = \left(\frac{C}{C_A} \right)^2 T_{RA} \tag{21S}$$

The mean transition times for $\mathbf{O} \leftrightharpoons \mathbf{I}$ and $\mathbf{R} \leftrightharpoons \mathbf{I}$ branches of the model can be derived

using the same analogy and are given as

$$T_{OI} = \left(\frac{C}{C_O}\right)^2 \left(\frac{1}{k_{45}^{flux} C^5} + \frac{1}{k_{34}^{flux} C^4} + \frac{1}{k_{23}^{flux} C^3}\right) \tag{22S}$$

$$T_{IO} = \left(\frac{C}{C_I}\right)^5 \left(\frac{C_O}{C}\right)^2 T_{OI} \tag{23S}$$

$$T_{RI} = \frac{1}{\hat{k}_{01}^{flux} C} + \frac{1}{\hat{k}_{12}^{flux} C^2} + \frac{1}{\hat{k}_{23}^{flux} C^3} + \frac{1}{\hat{k}_{34}^{flux} C^4} + \frac{1}{\hat{k}_{45}^{flux} C^5} \tag{24S}$$

$$T_{IR} = \left(\frac{C}{C_I}\right)^5 T_{RI} \tag{25S}$$

The $\hat{\cdot}$ in equation (24S) is used to distinguish the flux parameters in $\mathbf{R} \leftrightharpoons \mathbf{I}$ branch from $\mathbf{R} \leftrightharpoons \mathbf{O}$ and $\mathbf{O} \leftrightharpoons \mathbf{I}$ branches.

The mean open time for this model is given by:

$$\tau_O = \frac{1}{K_{OA} + K_{OI}} \tag{26S}$$

where K_{OA} and K_{OI} are the rates from the **O** state to **A** and **I** respectively. The rate K_{OA} is Ca^{2+} independent. Under optimal conditions most of the closing transitions in a patch clamp are between **O** and **A**. Thus we can approximate K_{OA} by τ_O^{-1} without introducing large error. i.e.

$$T_{OA} = \tau_O \tag{27S}$$

We can write the mean time from **O** to **A** as

$$\begin{aligned} T_{OA} = \text{Occupancy of } \mathbf{O} \times \frac{1}{\text{probability flux from } \mathbf{O} \text{ to } \mathbf{A}} \\ = K_O C^2 \times \frac{1}{k_{22}^{flux} C^2} \end{aligned} \tag{28S}$$

where k_{22}^{flux} is flux parameter for $\mathbf{A} \leftrightharpoons \mathbf{O}$ transition. Equation (28S) gives $k_{22}^{flux} = K_O/\tau_O$. In analogy with equation (28S), we can write

$$T_{AO} = \tau_O \frac{C_O^2}{C_A^2} \tag{29S}$$

It is easy to check that the product of times around the loop in one direction equals the product of times around in the opposite direction, confirming that detailed balance is satisfied. The transition rates, K_{ij}, between the various states (**R, A, O, I**) are the inverses of mean transition times, T_{ij} between states so that $K_{AR} = T_{AR}^{-1}$, etc. Various constants used in the above equations are derived as follows.

1.3 Parameters Estimation

We estimated various constants used in the mean transition times from the $P_{\mathbf{O}}$ and rapid perfusion experiments [4]. The $P_{\mathbf{O}}$ data gave us estimates to C_A, C_O, and C_I. $\tau_o = 30\ ms$ is the mean open time of the channel under optimal conditions (2 μM Ca^{2+} and 10 μM IP_3 concentrations). For the probability flux parameters $k_{ij}^{flux}s$ and $\hat{k}_{ij}^{flux}s$ we used the kinetic data on Ca^{2+} regulation at optimal IP_3 concentration ($10\mu M$) which is listed in the following chart [4].

$$\begin{aligned}
\text{Mean activation time (changing } Ca^{2+} \text{ from } < 10nM \text{ to } 2\mu M) &= 40 \pm 3ms \\
\text{Mean de-activation time (changing } Ca^{2+} \text{ from } 2\mu M \text{ to } < 10nM) &= 160 \pm 20ms \\
\text{Mean inhibition time (changing } Ca^{2+} \text{ from } 2\mu M \text{ to } 300\mu M) &= 290 \pm 40ms \\
\text{Mean inhibition-recovery time (changing } Ca^{2+} \text{ from } 300\mu M \text{ to } 2\mu M) &= 2.4 \pm 2s \\
\text{Changing } Ca^{2+} \text{ from } < 10nM \text{ to } 300\mu M, \frac{9}{103} &\text{ experiments failed to cause bursts} \\
\text{Changing } Ca^{2+} \text{ from } 300\mu M \text{ to } < 10nM, \frac{6}{94} &\text{ times the channel bursts before} \\
&\text{getting de-activated.}
\end{aligned} \tag{30S}$$

Thus we can write

$$T_{RA}\,|_{C=2\mu M} = 40ms \tag{31S}$$

$$T_{AR}\,|_{C=10nM} = 160ms \tag{32S}$$

$$T_{OI}\,|_{C=300\mu M} = 290ms \tag{33S}$$

$$T_{IO}\,|_{C=2\mu M} = 2.4s \tag{34S}$$

$$\frac{T_{RA}}{T_{RI}}\,|_{C=300\mu M} = \frac{9}{103} \tag{35S}$$

$$\frac{T_{IR}}{T_{IO}}\,|_{C=10nM} = \frac{6}{94} \tag{36S}$$

Using the equalities 31S and 32S we extracted k_{01}^{flux} and k_{12}^{flux}. Equalities 33S and 34S gave us k_{23}^{flux} and k_{45}^{flux}. We put k_{34}^{flux} equal to one as this corresponds to the fast transition in the chain $\mathbf{O} \leftrightharpoons \mathbf{I}$. $\hat{k}_{01}^{flux}$ and $\hat{k}_{45}^{flux}$ are extracted from equalities 35S and 36S. Finally, we put $\hat{k}_{12}^{flux}$, $\hat{k}_{23}^{flux}$, and $\hat{k}_{34}^{flux}$ equal to 1 as they correspond to fast transitions between low occupancy states. The values of occupancy and probability flux parameters are given in Table 2S.

1.4 Stochastic Scheme of Channel Gating

The gating of IP_3R is given by the four state model described in the main text. To determine the state of the channel, we have to determine the transition probabilities at a given time. That is, if the j^{th} channel is in state i, we have to determine the probabilities with which it remains in that state or switches into another state allowed by the kinetic scheme shown in Fig. 1 (main text) within the time interval Δt. For example, if a channel is in state **R**; possible transitions are to states **A** and **I**. For a sufficiently small time interval Δt, the probabilities for these transitions are given by $P_{R\to A}^{(j)} = K_{RA}^{(j)}\Delta t$ and $P_{R\to I}^{(j)} = K_{RI}^{(j)}\Delta t$. The probability for the channel to remain in state **R** is $P_{R\to R} = 1 - P_{R\to A} - P_{R\to I}$. To determine the transition probabilities, we followed the procedure outlined in part by the Gillespie algorithm [5]. The unit interval is divided into three subintervals of length $P_{R\to i}\Delta t$, i represent the three states to which the channel can make transition. If a random number drawn from a uniform distribution over the unit interval falls into the subinterval $P_{R\to i}\Delta t$, the corresponding transition is performed. The time interval Δt was kept small enough for the linear dependence of $P_{i\to i}$ on the time interval to remain valid. We used a time step of 10 μs throughout this paper. The channel is open only when it is in state **O**. The above

procedure was repeated for all channels.

1.5 Diffusion of Ca^{2+} and Buffers

Ca^{2+} concentration on the cytoplasmic side of the cluster is controlled by diffusion; the flux coming out from the **ER** through IP_3Rs, J_j; and the concentrations of free stationary buffers, free mobile buffers and free dye: b_s, b_m and b_d, respectively. Thus the rate equations for Ca^{2+} concentration at distance r_j and time t due to channel j, $c^j(r_j,t)$; and free Ca^{2+} buffers, $b_s^j(r_j,t)$; $b_m^j(r_j,t)$; and $b_d^j(r_j,t)$ at distance r_j and time t from channel j are described as below:

$$\begin{aligned}
\frac{\partial c^j(r_j,t)}{\partial t} &= D_c\nabla_j^2 c_j + J_j\delta(r_j) + k_s^r(B_s - b_s^j) - k_s^f c^j b_s + k_m^r(B_m - b_m^j) - k_m^f c^j b_m^j \\
&\quad + k_d^r(B_d - b_d^j) - k_d^f c^j b_d^j \qquad (37S)\\
\frac{\partial b_s^j}{\partial t} &= k_s^r(B_s - b_s^j) - k_s^f c^j b_s^j \qquad (38S)\\
\frac{\partial b_m^j}{\partial t} &= D_m\nabla_j^2 b_m^j + k_m^r(B_m - b_m^j) - k_m^f c^j b_m^j \qquad (39S)\\
\frac{\partial b_d^j}{\partial t} &= D_d\nabla_j^2 b_d^j + k_d^r(B_d - b_d^j) - k_d^f c^j b_d^j. \qquad (40S)
\end{aligned}$$

In the above equations B_i is the total concentration, k_i^f the forward (binding) rate, and k_i^r reverse (unbinding) rate for the various buffers with $i = s, m, d$. D_c, D_m, and D_d are the diffusion coefficients for Ca^{2+} , mobile buffers, and dye respectively. We consider slow mobile buffer mimicking ethylene glycol tetraacetic acid (EGTA). The term "slow" refer to binding kinetics of buffer, not its mobility. We also include ATP as a mobile Ca^{2+} buffer [6]. $\delta(r_j)$ is the Dirac delta function and J_j is the Ca^{2+} flux through the j^{th} channel.

$$J_j = \begin{cases} \frac{I}{2\times F\times \delta V} & \text{for } r \le \Delta r, \\ 0 & \text{for } r > 0. \end{cases} \qquad (41S)$$

Where $I = 0.075\ pA$ is the channel current, F is the Faraday's constant, $\Delta r = 5nm$, and δV is the volume of the hemisphere over the channel having a radius of r_{pore} [7]. Using $I = 0.075\ pA$ in Eq. (41S), a channel experiences approximately 300 μM Ca^{2+} when open [8]. As we will discuss in the main text, smaller value of I gives rise to puffs with much longer lifetime than those observed experimentally. We assume that the Ca^{2+} pump and leak

currents are slow on the time scales considered here and therefore have negligible effects. Various parameters used in Eqs. (37S-40S) are given in Table 3S.

1.6 Elements of Tridiagonal Matrix (TM)

Here we derive the elements of the TM for equations (37S-40S). In what follows n is the time index and j is the space index in spherical polar coordinates. We can write equation (6) as

$$\begin{aligned}\frac{c^{(n+1)}-c^{(n)}}{\Delta t} &= D\nabla^2 c^{(n+1)} + J\delta(r) + k_s^r(B_s - b_s^{(n)}) - k_s^f c^{(n+1)} b_s^{(n)} \\ &\quad + k_m^r(B_m - b_m^{(n)}) - k_m^f c^{(n+1)} b_m + k_d^r(B_d - b_d^{(n)}) \\ &\quad - k_d^f c^{(n+1)} b_d^{(n)} \end{aligned} \tag{42S}$$

Writing the Laplacian in spherical polar coordinates and considering no-flux boundary conditions we get the elements of lower, middle, and upper diagonal (a_j, b_j, and c_j respectively) of the TM given as

$$a_j = \begin{cases} 0 & \text{if } j = 1 \\ \frac{-D\Delta t}{\Delta r^2}(1-\frac{1}{2j})^2 & \text{if } j = 2, ...N-1 \\ \frac{-2D\Delta t}{\Delta t} & \text{if } j = N. \end{cases} \tag{43S}$$

$$b_j = \begin{cases} \frac{6D\Delta t}{\Delta r^2} + 1 + k_s^f b_s^{(n,j)}\Delta t + k_m^f b_s^{(n,j)}\Delta t + k_d^f b_d^{(n,j)}\Delta t & \text{if } j = 1 \\ \frac{D\Delta t}{\Delta r^2}(1+\frac{1}{2j})^2 + \frac{D\Delta t}{\Delta r^2}(1-\frac{1}{2j})^2 + 1 + k_s^f b_s^{(n,j)}\Delta t & \\ + k_m^f b_s^{(n,j)}\Delta t + k_d^f b_d^{(n,j)}\Delta t & \text{if } j = 2, ..N-1 \\ \frac{2D\Delta t}{\Delta r^2} + 1 + k_s^f b_s^{(n,j)}\Delta t + k_m^f b_s^{(n,j)}\Delta t + k_d^f b_d^{(n,j)}\Delta t & \text{if } j = N. \end{cases} \tag{44S}$$

$$c_j = \begin{cases} \frac{-6D\Delta t}{\Delta r^2} & \text{if } j = 1 \\ \frac{-D\Delta t}{\Delta r^2}(1+\frac{1}{2j})^2 & \text{if } j = 2, ...N-1 \\ 0 & \text{if } j = N. \end{cases} \tag{45S}$$

The right hand side for the TM system for the cytosolic Ca^{2+} concentration is represented by d_j and is

$$d_j = c^{(n,j)} + k_s^r(B_s - b_s^{(n,j)})\Delta t + J\delta(r)\Delta t + k_m^r(B_m - b_m^{(n,j)})\Delta t \\ + k_d^r(B_d - b_d^{(n,j)})\Delta t, \text{ j=1,..N} \tag{46S}$$

The rate equations for mobile and dye buffers can be expanded and solved iteratively in similar fashion.

The stationery buffers can be solved iteratively according to

$$\frac{b_s^{(n+1,j)} - b_s^{(n,j)}}{\Delta t} = k_s^r(B_s - b_s^{(n+1,j)}) - k_s^f c^{(n,j)} b_s^{(n+1,j)} \tag{47S}$$

$$b_s^{(n+1,j)} = \frac{b_s^{(n,j)} + k_s^r B_s \Delta t}{1 + k_s^f c^{(n,j)}\Delta t + k_s^r \Delta t} \tag{48S}$$

1.7 Fluorescence Estimation

We estimate the fluorescence signal from total internal reflection fluorescence (TIRF) microscopy by following the procedure outlined in [9], i.e.

$$Fluorescence = \sum_j \int\int\int dxdydz b_d^{*j}(r_j(x,y,z)) \\ \times\Big(-\frac{(x-x_0)^2}{\sigma_x^2} - \frac{(y-y_0)^2}{\sigma_y^2}\Big) exp\Big(-\frac{z}{\gamma_z}\Big) \tag{49S}$$

Where $b^{*j} = (B_d - b_d^j)$ is the Ca^{2+}-bound dye due to the Ca^{2+} released by the j^{th} channel, $\sigma_x^2 = \sigma_y^2 = 0.0225\ \mu m^2$, $\gamma_z = 0.15\ \mu m$, and $x_0, y_0 = 0$. The integration in Eq. (49S) is performed over a cubic volume of $1\ \mu m \times 1\ \mu m \times 0.15\ \mu m$.

1.8 Experimental Methods

The experimental data in the main text shown for comparison is taken from [10, 11]. The $P_{\mathbf{O}}$ data is taken from [10] and the puff data is taken from [11]. Here we briefly present the experimental methods used to acquire those data, and refer the reader for detailed description to [10, 11].

1.8.1 $P_{\mathbf{O}}$ data [10]

Patch clamp of the outer membrane of individual nuclei mechanically isolated from *Xenopus Laevis* oocytes was performed as described in [12]. The cytoplasmic aspect of the IP_3R channel faced into the patch pipette. All experimental solutions contained 140 mM KCl, 10 mM Hepes (pH adjusted to 7.1 with KOH), and 0 or 0.5 mM Na_2ATP as indicated. Total Ca^{2+} content in the solutions was determined by induction-coupled plasma mass spectrometry (Mayo Medical Laboratory, Rochester, MN). Free Ca^{2+} concentrations were calculated by using the MAXCHELATOR software (C. Patton, Stanford University, Palo Alto, CA). Pipette solutions contained 10 μM concentration of IP3. All experiments were performed at room temperature with the pipette electrode at +20 mV relative to the reference-bath electrode. Each data point shown is the mean of results from at least four separate patch-clamp experiments performed under the same conditions. Error bars indicate the standard error of the mean (SEM). Single-channel currents were amplified by an Axopatch-1D amplifier (Axon Instruments, Foster City, CA), filtered at 1 kHz, digitized at 5 kHz. Channel dwell times and $P_{\mathbf{O}}$s were obtained by using TAC 3.03 (Bruxton, Seattle, WA).

1.8.2 Puff data [11]

Human neuroblastoma SH-SY5Y cells were cultured as described in [13] in a mixture (1:1) of Hams F12 medium and Eagle MEM, supplemented with 10% (vol./vol.) FCS and 1% nonessential amino acids. Cells were incubated at 37 ^{o}C in a humidified incubator gassed with 95% air and 5% CO_2, passaged every 7 days, and used for a maximum of 20 passages. Four days before imaging, cells were harvested in PBS solution without Ca^{2+} or Mg^{2+} and subcultured in Petri dishes with glass coverslips as the base (MatTek) at a seeding density of 3×10^4cells/mL. Cells were then loaded a few hours before use by incubation with Hepes-buffered saline solution (in mM: NaCl, 135; KCl, 5; $MgSO_4$, 1.2; $CaCl_2$, 2.5; Hepes 5; glucose, 10) containing 1 μM ci-IP_3 / PM (SiChem) at room temperature for 45 min, followed by incubation with 1 μM caged ci-IP_3 /PM plus 5 μM fluo-4 AM (Invitrogen) at room temperature for 45 min, and finally 45 min with 5 μM EGTA-AM (Invitrogen).

Imaging of changes in Ca^{2+} was accomplished by using a home-built TIRF microscope system based around an Olympus IX 70 microscope equipped with an Olympus X60 TIRFM objective (NA 1.45). Fluorescence of cytosolic fluo-4 was excited within the $\approx$ 100-nm evanescent field formed by total internal reflection of a 488-nm laser beam incident through the microscope objective at the cover glass/aqueous interface. Images of emitted fluorescence $\lambda > 510$ nm were captured at a resolution of 128×128 pixels (1 pixel=0.33 μm) at a rate of

420 frames/s by a Cascade 128 electronmultiplied CCD camera (Roper Scientific). Photorelease of i-IP_3 from a caged precursor was evoked by flashes of UV light (350 - 400 nm) derived from a fiber-optic arc lamp source introduced via a UV reflecting dichroic mirror in the upper side-port of the microscope. The UV light was adjusted to uniformly irradiate a region slightly larger than the imaging frame, and any given imaging field was exposed to only a single flash. We sought to obtain data under condition of roughly constant cytosolic IP_3, and adjusted the flash duration as required between 50 and 400 ms so as to obtain a similar mean puff frequency (≈ 1 per s/cell) in each cell to compensate for variations in loading of caged IP_3. Image processing and analysis was done using MetaMorph 7.5 (Molecular Dynamics).

References

[1] G. Schwarz, Estimating the dimension of a model, The Annals of Statistics 6 (1978) 461–464.

[2] W. Bruno, J. Yang, J. Pearson, Using independent open-to-closed transitions to simplify aggregated Markov models of ion channel gating kinetics, Proc. Natl. Acad. Sci. USA 102 (2005) 6326.

[3] J. Yang, W. J. Bruno, W. S. Hlavacek, J. E. Pearson, On imposing detailed balance in complex reaction mechanisms, Biophys. J. 91 (2006) 1136–1141.

[4] D. O. D. Mak, J. E. Pearson, K. H. Cheung, S. Datta, M. Fernandez-Mongil, K. J. Foskett, Rapid ligand-regulated gating kinetics of single IP_3R Ca^{2+} release channels, EMBO Reports 8 (2007) 1044–1051.

[5] D. Gillespie, A general method for numerically simulating the stochastic time evolution of coupled chemical reactions, J. Comp. Phy. 22 (1976) 403–434.

[6] S. Baylor, S. Hollingworth, Model of sarcomeric Ca^{2+} movements, including ATP Ca^{2+} binding and diffusion, during activation of frog skeletal muscle, J. Gen. Physiol. 112 (1998) 297.

[7] J. Shuai, J. Pearson, K. J. Foskett, D. O. D. Mak, I. Parker, A kinetic model of single and clustered IP_3 receptors in the absence of Ca^{2+} feedback, Biophys. J. 93 (2007) 1151–1162.

[8] R. Thul, M. Falcke, Release currents of IP_3 receptor channel clusters and concentration profiles, Biophys. J. 86 (2004) 2660–2673.

[9] J. Shuai, I. Parker, Optical single-channel recording by imaging Ca^{2+} flux through individual ion channels: theoretical considerations and limits to resolution, Cell Calcium 37 (2005) 283–299.

[10] D. O. D. Mak, S. McBride, K. J. Foskett, IP_3 activation of IP_3R Ca^{2+} channel by ligand tuning of Ca^{2+} inhibition., Proc. Natl. Acad. Sci. USA 95 (1998) 15821–15825.

[11] I. F. Smith, I. Parker, Imaging the quantal substructure of single IP_3R channel activity during Ca^{2+} puffs in intact mammalian cells, Proc. Natl. Acad. Sci. USA 106 (2009) 6404–6409.

[12] D. O. D. Mak, K. J. Foskett, Single-channel kinetics, inactivation, and spatial distribution of ip$_3$rs in xenopus oocyte nucleus, J. Gen. Physiol. 109 (1997) 571.

[13] I. Smith, S. Wiltgen, I. Parker, Localization of puff sites adjacent to the plasma membrane: functional and spatial characterization of Ca^{2+} signaling in SH-SY5Y cells utilizing membrane-permeant caged IP_3, Cell Calcium 45 (2009) 65–76.

[14] M. Falcke, Reading the patterns in living cells-the physics of Ca^{2+} signaling, Adv. Phy. 53 (2004) 255–440.

[15] E. Neher, G. Augustine, Ca^{2+} gradients and buffers in bovine chromaffin cells., J. Physiol. 450 (1992) 273–301.

[16] Z. Zhou, E. Neher, Mobile and immobile Ca^{2+} buffers in bovine adrenal chromaffin cells, J. Physiol. 469 (1993) 245–273.

[17] A. Williams, D. West, R. Sitsapesan, Light at the end of the Ca^{2+}-release channel tunnel: structures and mechanisms involved in ion translocation in ryanodine receptor channels, Quart. Rev. Biophys. 34 (2001) 61–104.

[18] C. Taylor, P. da Fonseca, E. Morris, IP_3 receptors: the search for structure, Tren. Biochem. Sci. 29 (2004) 210–219.

[19] S. Zeller, S. Rüdiger, H. Engel, J. Sneyd, G. Warnecke, I. Parker, M. Falcke, Modeling the modulation by buffers of Ca^{2+} release through clusters of IP_3 receptors, Biophys. J. 97 (2009) 992–1002.

[20] N. Allbritton, T. Meyer, L. Stryer, Range of messenger action of Ca^{2+} ion and IP_3, Genes Dev. 4 (1990) 1753.

[21] S. Dargan, I. Parker, Buffer kinetics shape the spatiotemporal patterns of IP_3-evoked Ca^{2+} signals, J. Physiol. 553 (2003) 775–788.

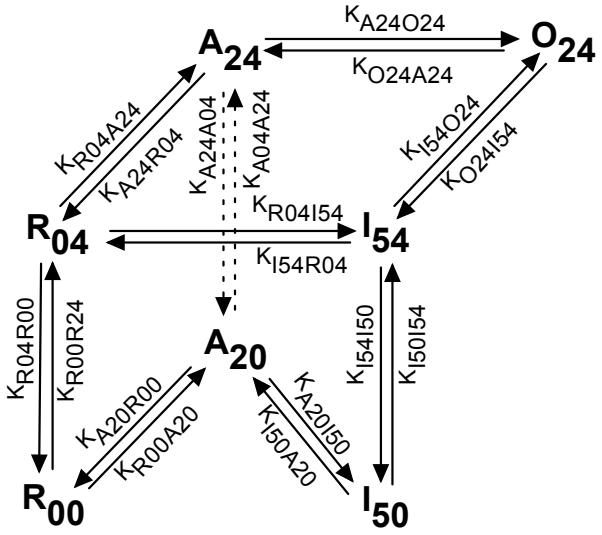

Fig. 1S: Schematic of the seven state model for single IP_3R channel. **Xij** represents the state where the channel has **i** Ca^{2+} and **j** IP_3 bound. K_{XijYmn} represents the transition rate from state **Xij** to **Ymn**. The occupancy parameter, K_{Xij} of state **Xij** is the product of all forward equilibrium constants for the reactions along an arbitrary path connecting state **Xij** to **R00**. For example, $K_{R04} = \frac{K_{R00R04}}{K_{R04R00}}$, $K_{A24} = \frac{K_{R00R04}}{K_{R04R00}} \frac{K_{R04A24}}{K_{A24R04}}$, etc.

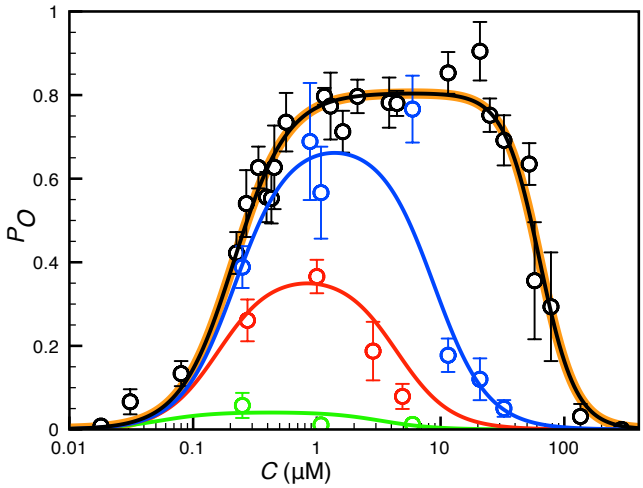

Fig. 2S: Equilibrium open probability of the single IP_3R channel in *Xenopus laevis* oocytes as a function of C at four IP_3 concentrations (10 μM black, 33 nM blue, 20 nM red, 10 nM green). The solid lines and circles represent the fit from the seven state model and the mean P_O from patch clamp experiments on *Xenopus Laevis* occytes [10] respectively. The error bars represent standard errors of the mean. The thick orange line is the P_O from the four state model at 10 μM and is shown for comparison.

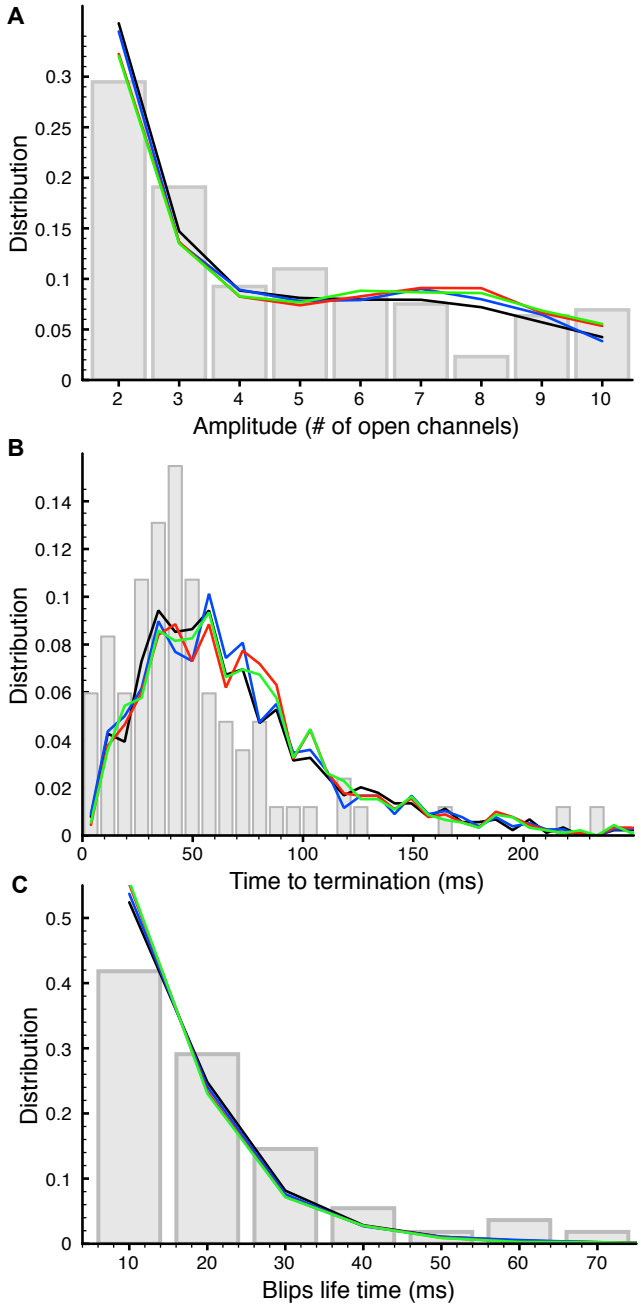

Fig. 3S: Statistics of Ca^{2+} puffs and blips in the presence of various buffer concentrations: Distribution of (A) puffs amplitude, (B) puffs termination time, and (C) blips life time. The distributions given by the model are obtained from the number of open channels during elementary Ca^{2+} release events using buffer concentrations of $B_s = 100\ \mu M, B_{EGTA} = 100\ \mu M$ (black line), $B_s = 50\ \mu M, B_{EGTA} = 100\ \mu M$ (blue line), $B_s = 0\ \mu M, B_{EGTA} = 100\ \mu M$ (red line), $B_s = 0\ \mu M, B_{EGTA} = 0\ \mu M$ (green line). The gray bars represent experimental data and is modified from [11].

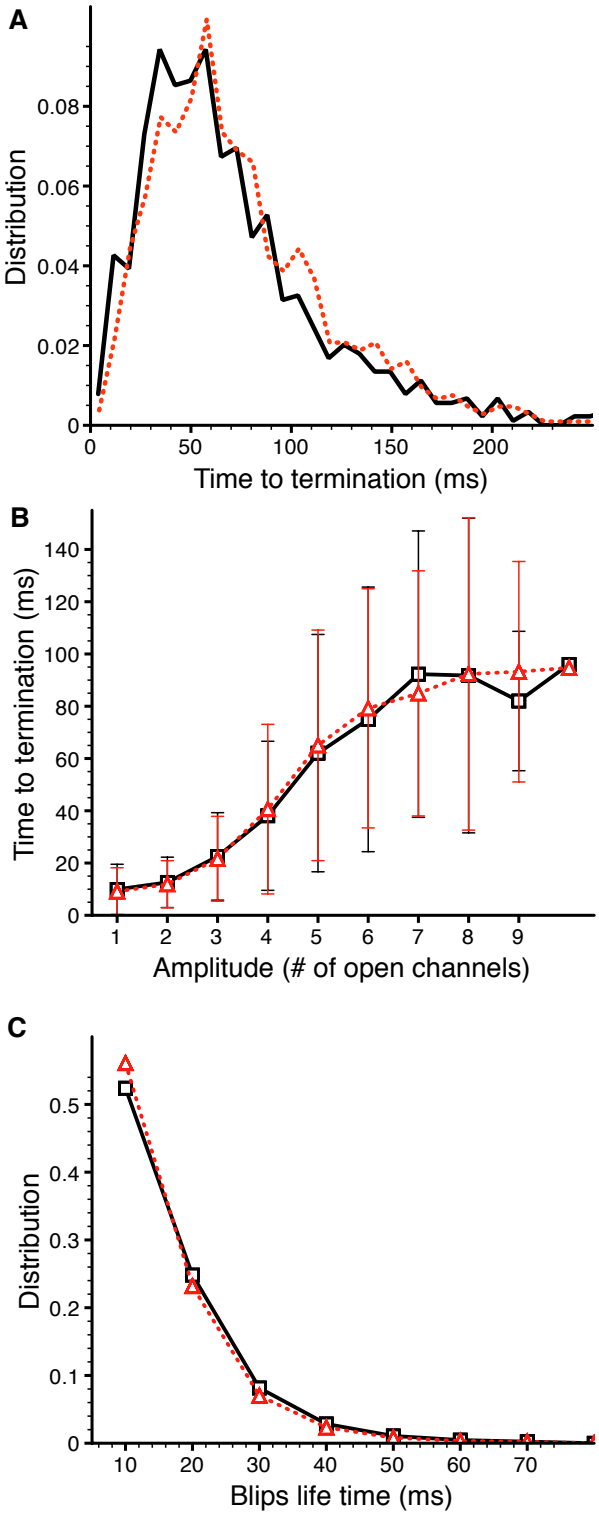

Fig. 4S: Statistics of Ca^{2+} puffs and blips in the presence of 0 μM (solid lines) and 200 μM (dotted lines) ATP: (A) Distribution of puff termination times, (B) termination time as a function of puff amplitude, and (C) life time distribution of blips.

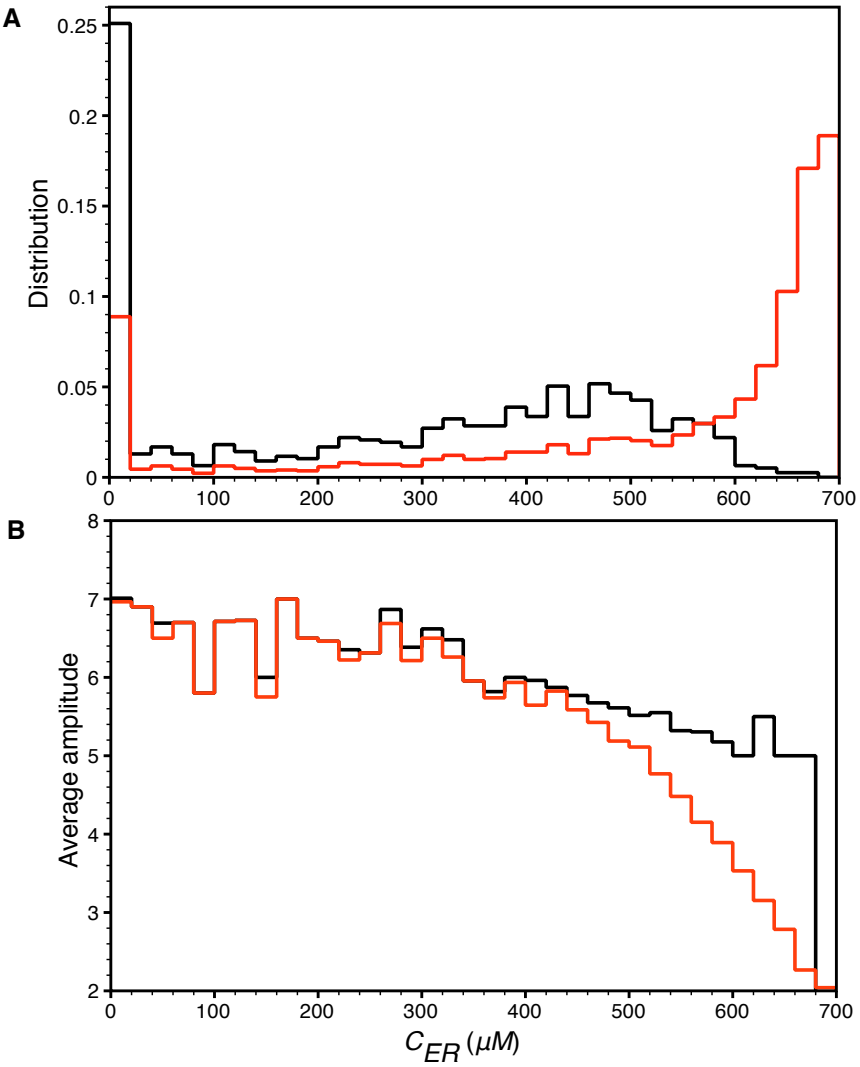

Fig. 5S: Bigger puffs have higher probability of depleting **ER**. (A) Distribution of local **ER** Ca^{2+} concentration for C_{ER}^{rest} = 700 μM. The black and red lines correspond to the puffs with $5 \leq Amplitude \leq 10$ and $2 \leq Amplitude \leq 10$ respectively. The distribution shifts to the right when smaller puffs are taken into account indicating that bigger puffs are more likely to deplete **ER**. (B) Average amplitude (number of open channels) of puffs for each bin in panel (A) showing that puffs causing lower **ER** Ca^{2+} have higher average amplitude and vice versa. The line colors in panel (B) have the same meaning as in (A).

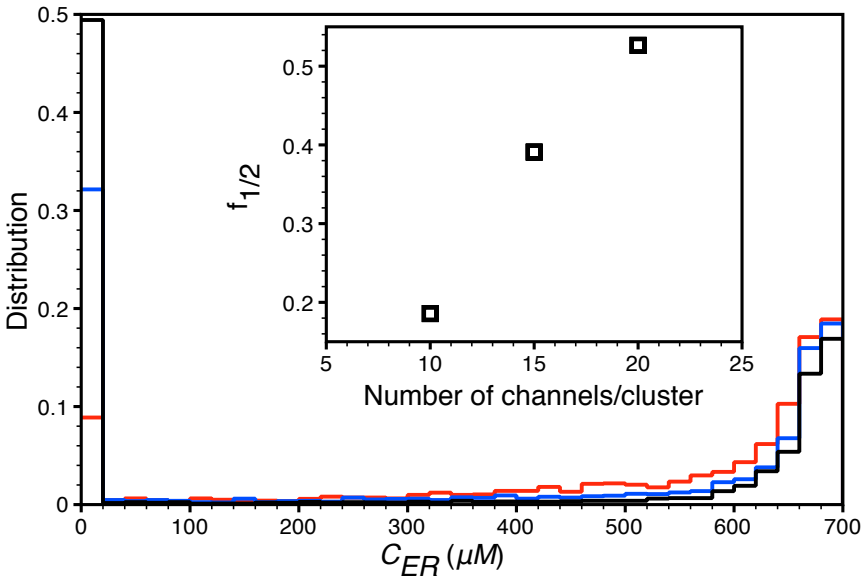

Fig. 6S: Bigger clusters have higher probability of depleting **ER**. Distribution of local **ER** Ca^{2+} concentration for puffs produced by a cluster of 10 (red), 15 (blue), and 20 (black) channels. All puffs ($Amplitude > 2$) were taken into account and C_{ER}^{rest} = 700 μM. The distribution shifts to the left as the number of channels in the cluster increases indicating that bigger clusters are more likely to deplete **ER**. In all three cases, channels were arranged in a two-dimensional array with an inter-channel spacing of 120 nm as described in the main text. The inset shows the fraction of times when the C_{ER} dropped below 50% of C_{ER}^{rest} (350 μM) as a function cluster size.

Table 1S: Occupancy parameters for the seven state model.

Parameter	Value
K_{R00}	1
K_{A20}	$1.035 \times 10^5 \mu M^{-2}$
K_{I50}	$1 \times 10^4 \mu M^{-4}$
K_{R04}	$3.11 \times 10^{10} \mu M^{-4}$
K_{A24}	$1.135 \times 10^{11} \mu M^{-6}$
K_{O24}	$4.56 \times 10^{11} \mu M^{-6}$
K_{I54}	$2.296 \times 10^6 \mu M^{-9}$

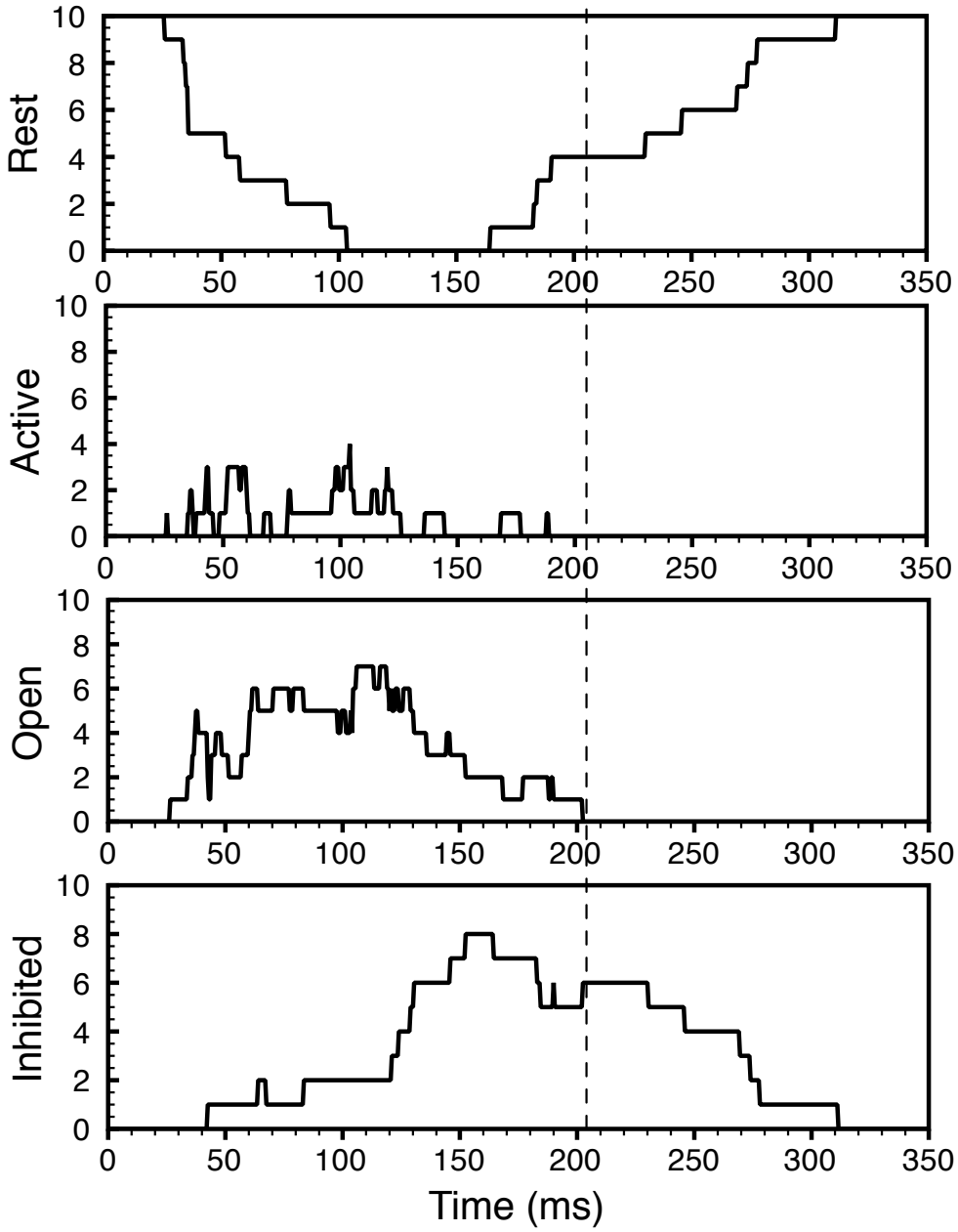

Fig. 7S: Puff cycle. The number of channels in each of the four states during a single puff. The dashed line after 200 ms marks the puff termination.

Table 2S: Gating parameters for the four state model.

Parameter	Value
τ_O	$30ms$
C_A	$0.484\mu M$
C_O	$0.238\mu M$
C_I	$6.5\mu M$
k_{01}^{flux}	$0.0162/\mu Mms$
k_{12}^{flux}	$0.027/\mu M^2ms$
k_{23}^{flux}	$2.1651 \times 10^{-4}/\mu M^3ms$
k_{34}^{flux}	$1.0/\mu M^4ms$
k_{45}^{flux}	$3.5935 \times 10^{-8}/\mu M^5ms$
$\hat{k}_{01}^{flux}$	$0.0014127/\mu Mms$
$\hat{k}_{12}^{flux}$	$1.0/\mu M^2ms$
$\hat{k}_{23}^{flux}$	$1.0/\mu M^3ms$
$\hat{k}_{34}^{flux}$	$1.0/\mu M^4ms$
$\hat{k}_{45}^{flux}$	$5.6297 \times 10^{-7}/\mu M^5ms$

Table 3S: Concentrations, rates, and cluster parameters

Quantity	Symbol	—	Numerical Value	Reference
Concentrations				
Resting Cytosolic Calcium	Ca_{rest}	=	$50nM$	[14]
Lumenal Calcium	Ca_{ER}	=	$700\mu M$	[8]
Cytosolic Ca^{2+} in Front of Open Pore	C_{max}	=	$300\mu M$	
Optimal Ca^{2+}	C_{opt}	=	$2\mu M$	
Stationary Buffer	B_s	=	$100\mu M$	[15, 16]
Dye Buffer	B_d	=	$25\ \mu M$	
EGTA	B_{EGTA}	=	$100\ \mu M$	
ATP	B_{ATP}	=	0, unless mentioned otherwise	
Channel Scales				
Number of channels	N_{ch}	=	$10-20$	[11]
Pore Radius	r_{pore}	=	$2.5nm$	[17, 18]
IP_3R Radius	R_{IPR}	=	$10nm$	[19]
Mean Nearest Neighbor Channel Spacing	r_{nn}	=	$120nm$	
Diffusion Coefficients				
Ca^{2+}	D_c	=	$0.223\mu m^2/ms$	[20]
Dye	D_d	=	$0.200\mu m^2/ms$	[21]
EGTA	D_{EGTA}	=	$0.200\mu m^2/ms$	[21]
ATP	D_{ATP}	=	$0.14\mu m^2/ms$	[6]
Rates				
Stationary Buffer	k_s^f	=	$0.2/\mu Mms$	[14]
	k_s^r	=	$0.4/ms$	[14]
Dye Buffer	k_d^f	=	$0.1/\mu Mms$	[14, 21]
	k_d^r	=	$0.025/ms$	[14, 21]
EGTA	k_{EGTA}^f	=	$0.006/\mu Mms$	[14, 21]
	k_{EGTA}^r	=	$0.001/ms$	[14, 21]
ATP	k_{ATP}^f	=	$0.01364/\mu Mms$	[6]
	k_{ATP}^r	=	$30/ms$	[6]